

Influence of variable bifurcation angulation and outflow boundary conditions in 3D finite element modelling of left coronary artery on coronary diagnostic parameter

Kalimuthu Govindaraju^{1,*}, Irfan Anjum Badruddin², Girish N. Viswanathan³, Sarfaraz Kamangar², N. J. Salman Ahmed⁴ and Abdullah A. A. Al-Rashed⁵

¹Centre for Engineering Programs, HELP College of Arts and Technology, Kuala Lumpur, Malaysia

²Department of Mechanical Engineering, University of Malaya, Malaysia

³Consultant Interventional Cardiologist, Derriford Hospital, Plymouth, UK

⁴Centre for Energy Sciences, Department of Mechanical Engineering, University of Malaya, Kuala Lumpur, Malaysia

⁵Department of Automotive and Marine Engineering Technology, College of Technological Studies, The Public Authority for Applied Education and Training, Kuwait

Theoretical impact of left coronary bifurcation angulation (BA) variations and percentage of flow distribution variations (FDV) in coronary artery branches (CAB) on anatomic assessment of bifurcated lesions, is investigated by considering fractional flow reserve (FFR) as a standard diagnostic parameter. According to Medina classification, computational models of coronary bifurcation lesions types of (1, 0, 0), (0, 1, 0) and (0, 0, 1) were developed. The models included BA of 30°, 45°, 60°, 75°, 90° and 120°. Computational fluid dynamics analysis was performed under hyperaemic flow condition and FFR was evaluated with percentage of FDV in CAB. For any fixed percentage of flow in the CAB and change in BA, FFR was significantly affected in the lesion type (1, 0, 0) whereas no significance was found in the lesion types (0, 1, 0) and (0, 0, 1). Percentage of FDV in CAB for any fixed BA significantly altered FFR in all the lesion types. Overall, 5%, 41% and 73% variations in FFR were found in (1, 0, 0), (0, 1, 0) and (0, 0, 1) respectively. The variation of BA could not be neglected in *in vitro* anatomical assessment for lesion type (1, 0, 0) but not in case of (0, 1, 0) and (0, 0, 1). Nevertheless, percentage of FDV in CAB is significantly altered FFR in the left coronary bifurcation lesions, which lead to underestimation of stenosis severity and postponement of coronary interventional procedure.

Keywords: Bifurcation angulation, computational fluid dynamics, coronary branch flow, FFR, left coronary artery.

FROM clinical practice, coronary artery bifurcations are regions where the flow is strongly disturbed, which is a potential risk for development of atherosclerotic lesions at the site of branching^{1,2}. An artery bifurcation plays a key role in pressure distribution, where side-branches

steal flow from the main vessel similar to collaterals. Left coronary artery (LCA) has short left main stem (LMS) and quickly divides into left anterior descending (LAD) and left circumflex (LCX) with an angle between them^{1,3}. The angle between these two coronary branches differs in dimension and shape from person to person. There is a direct correlation between coronary angulations and subsequent haemodynamic changes¹. Variations in LCA angles disturb flow pattern and prone to change the wall pressure and shear stress gradient^{1,4}.

A bifurcation lesion is the narrowing of coronary artery that may occur in LMS, in LAD and/or in LCX⁵. Medina *et al.*⁶ proposed a simple bifurcation lesion classification consisting of a binary value (1, 0). Any narrowing with critical stenosis of 50% and above in any segment receives a binary value 1; otherwise, binary value 0 is assigned starting from left to right. The three suffixes are separated by commas⁷.

Recent studies on effect of plaque distributed in the left coronary bifurcation have shown that plaque distribution has a direct effect on flow parameters at stenotic locations^{8,9}. Murray¹⁰ predicted the percentage of distribution of total flow rate through side branches (SB), by correlating flow ratio through SB, with ratio of the diameter of SB to the third power. Groen *et al.*¹¹ showed that Murray's law can be reasonably applied when the percentage of area stenosis is ≤ 65 , whereas for stenosis $\geq 66\%$ it is inadequate in predicting the flow ratio at the bifurcation.

Coronary bifurcation lesions have been one of the most challenging lesion subsets in the field of percutaneous coronary intervention (PCI)¹². Anatomic severity assessment of bifurcation lesions using angiography is limited due to vessel overlap, angulation and foreshortening¹³. Therefore, a standardized physiological assessment of bifurcation lesions is required, which can be done with fractional flow reserve (FFR)^{12,14,15} (ratio of distal coronary pressure to aorta pressure under hyperaemic condition).

*For correspondence. (e-mail: grajukm@gmail.com)

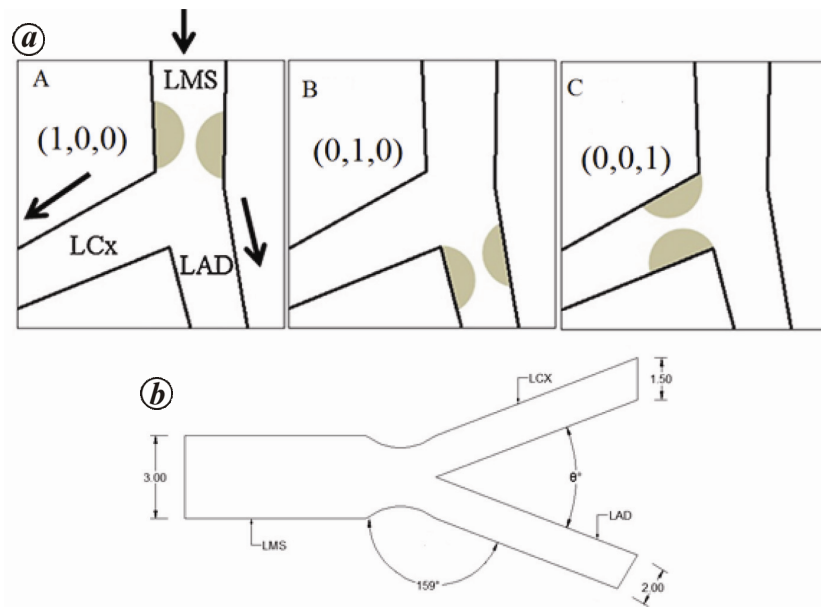


Figure 1. *a*, Schematic diagram of bifurcated artery with stenosis. *b*, Schematic diagram showing bifurcated artery geometry.

Numerous clinical trials revealed that in the presence of stenosis, $FFR < 0.75$ requires coronary intervention, whereas $FFR > 0.75$ defers revascularization^{16,17}. However, recent studies FAME 1 (fractional flow reserve versus angiography for multi-vessel evaluation 1) and FAME 2 use a clinically valid FFR cutoff value of 0.8 (ref. 18).

Since the coronary diagnostic parameter is derived from pressure measurements proximal and distal to the stenosis under hyperaemic flow condition, it is useful to study (i) variations of pressure measurements and hence FFR in the stenosed bifurcated coronary artery, (ii) variable angulations between LAD and (iii) LCX and variable flow through them using CFD analysis. It is expected that the geometry and flow through coronary artery branches (CAB) play a substantial role in evaluating physiological significance of stenosis severity for the bifurcated lesion.

Methodology

Stenosis geometry

To examine the influence of variable bifurcation angulation (BA) and percentage of flow distribution variation (FDV) in CAB on coronary diagnostic parameter, we considered 80% area stenosis (AS) (per cent AS = $100\% \times (\text{reference lumen area} - \text{minimum lumen area}) / \text{reference lumen area}$), which is located at three different configurations such as (1, 0, 0), (0, 1, 0) and (0, 0, 1) as shown in Figure 1 *a*. The angulation (θ) between LAD and LCX is taken as 30°, 45°, 60°, 75°, 90° and

120° keeping the angulation between LMS and LAD as 159°, to isolate the effect of a single geometric factor in all three configurations¹⁹, and the internal diameter of unobstructed LMS, LAD and LCX are 3, 2 and 1.5 mm respectively (Figure 1 *b*)¹.

Geometry of the stenosis considered for analysis is identical to that of the geometry described by Dash *et al.*²⁰, in the absence of a coaxial catheter (the stenosis developed in a concentric manner over a length of 10 mm), which is categorized as the cut-off lesion length for sensitive prediction index for the FFR value of 0.75 (ref. 21). The stenosis geometry was calculated as follows

$$\frac{\tilde{r}(\tilde{z})}{a} = 1 - \frac{h}{a} \sin \pi \left(\frac{\tilde{z} - d}{L} \right), \quad d \leq \tilde{z} \leq d + L, \quad (1)$$

where $\tilde{r}(\tilde{z})$ is the radius of lumen, a the radius of an unobstructed artery, \tilde{z} is along the artery axis, and h is the maximum projection of stenosis into the lumen. The throat diameters in configurations (1, 0, 0), (0, 1, 0) and (0, 0, 1) were 1.34, 1, 0.94 mm respectively. The LMS length proximal to stenosis was taken to be more than 15 times the LMS diameter for the flow to develop.

Computational blood flow modelling

Blood flow through coronary artery was assumed to be incompressible, unsteady, and governed by the Navier-Stokes equations as follows

$$\rho \left(\frac{\partial v}{\partial t} + v \cdot \nabla v \right) = \nabla \cdot \tau - \nabla P. \quad (2)$$

The continuity equation for incompressible flow is

$$\nabla \cdot \mathbf{v} = 0, \tag{3}$$

where \mathbf{v} is the 3D velocity vector, t time, ρ blood density, P pressure, and $\boldsymbol{\tau}$ the stress tensor. Blood was assumed to be non-Newtonian and followed the Carreau model²². Blood viscosity μ , given in poise (P) as a function of shear rate $\dot{\gamma}$ (in s^{-1}), was calculated as

$$\mu = \mu_\infty + (\mu_0 - \mu_\infty)[1 + (\lambda\dot{\gamma})^2]^{(n-1)/2}, \tag{4}$$

where $\lambda = 3.313$ s, $n = 0.3568$, $\mu_0 = 0.56P$ and $\mu_\infty = 0.0345$ P, and the density of the blood (ρ) was assumed to be 1050 kg/m^3 (ref. 23). A hybrid finite element/finite volume solver (ANSYSCFX V14.0) was used to discretize Navier–Stokes equations.

Meshing and boundary conditions

Computational domains were initially meshed with hexahedral elements as shown in Figure 2. The mesh elements are generated using ANSYS ICEM CFD version 14.0 (ANSYS, Inc. Canonsburg, PA, USA). The total number of elements varied from 250,000 to 300,000. Quality of mesh was checked by inspecting various parameters such as skewness, orthogonal quality and element quality.

A digitized data of transient parabolic velocity $u(t)$ ^{23,24} was applied at the inlet of LMS (Figure 3) to ensure that the 3D numerical analysis was a realistic simulation of *in vivo* conditions. No-slip condition was applied at the arterial wall in all three configurations under different branch angulations. The velocity profile for 80% AS was obtained from mean hyperaemic flow rate (\tilde{Q}) of 165 ml/min ^{23,25–27}.

There are two outflow boundaries for this problem. (i) percentage of flow distribution (FD) in CAB and (ii) stress-free boundary condition. Percentage of FD was set at the outlet of LAD and stress-free boundary conditions

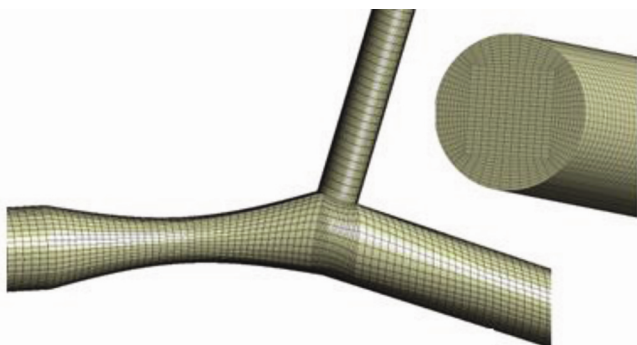


Figure 2. Computational mesh used for numerical study in the bifurcated stenotic artery model.

were set at the outlet of LCX²⁸ for configurations (1, 0, 0) and (0, 1, 0), whereas for configurations (0, 0, 1), percentage of FD was set at the outlet of LCX and stress-free boundary conditions were set at the outlet of LAD, in order to find the pressure downstream to the stenosis, which is an implicit result of the prediction of the numerical analysis²⁹. In configurations (1, 0, 0) and (0, 1, 0) the calculations were done for 70%, 80% and 90% of \tilde{Q} through LAD, whereas in configuration (0, 0, 1), 20%, 30% and 40% of \tilde{Q} through LCX were used to see the influence of outlet boundary conditions and BA, on pressure drop across the stenosis and hence the FFR. In all three configurations, a shear stress turbulence model was adopted as in our previous study³⁰.

Numerical methodology

A finite volume software CFX 14.0 (ANSYS CFX, Canonsburg, PA) was used for flow simulation. Adaptive time stepping method was used, wherein the initial time step was set at 0.001 s and minimum and maximum time steps were between 0.001 and 0.01 s. Increase and decrease in time step occurred after six target loops with factors of 1.5 and 0.1 respectively. Transient flow analysis was run for four cycles (0.8 s each) of pulsatile flow, with each time step converging to a residual target of 1×10^{-4} to ensure the periodic flow. In all cases, the guide wire was not considered. Subsequently, a mesh-independent study was performed with elements varying from 300,000 to 400,000 for discrepancies in pressure drop calculation and it was found that mesh convergence had been achieved. The mesh-independency test graph for the model (1, 0, 0) of 75° bifurcation with 70% of \tilde{Q} through LAD is shown in Figure 4. In this model, five

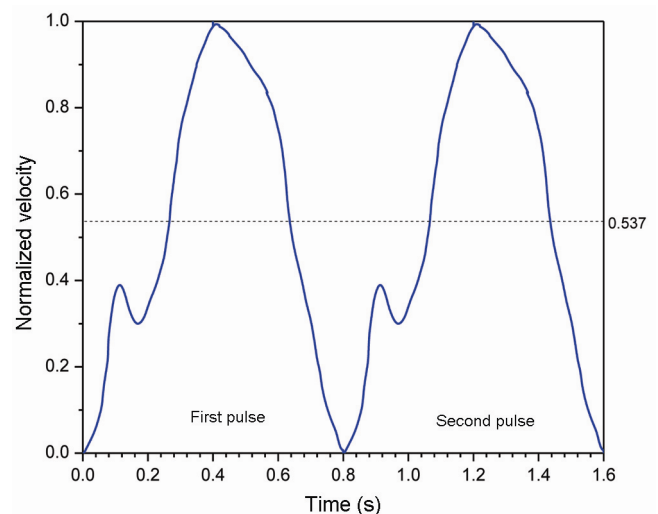


Figure 3. Normal coronary flow wave form \bar{u}/\bar{u}_{p-t} versus t (refs 23, 24). The peak diastolic velocity \bar{u}_{p-t} corresponds to a normalized velocity of 1.0, so that the ratio of mean to peak velocity \bar{u}/\bar{u}_{p-t} is 0.537.

grid systems with 251298, 288059, 311405, 330168 and 357931 were considered for pressure drop calculation. The difference in the pressure drop between the last two grid systems was 0.3%. So the fourth grid system was taken to compute FFR. Similarly mesh independency was tested in the rest of the models as well.

Pressure drop in bifurcated arteries

In all the bifurcated models, the overall time averaged pressure drop $\Delta\tilde{p} = \tilde{p}_a - \tilde{p}_d$ was obtained during cardiac cycles 3 and 4 where \tilde{p}_a and \tilde{p}_d are time averaged instantaneous pressures, measured proximal to the stenosis and at recovery region distal to the stenosis respectively³¹. No significant difference was found between $\Delta\tilde{p}$ values of cycles 3 and 4, thereby ensuring accuracy of numerical data reported for the third and fourth cycles.

In configuration (1, 0, 0), the \tilde{p}_a was measured at 3 mm proximal to the stenosis and \tilde{p}_d was measured at LAD, as it is the larger of the two branched vessels and supplies blood flow to a larger territory³². In configurations (0, 1, 0) and (0, 0, 1), \tilde{p}_d was measured distal to the stenosis in LAD and LCX respectively, and \tilde{p}_a was measured in LMS of both configurations at 3 mm before the arterial wall begins to bifurcate.

Diagnostic parameter

FFR: At hyperaemia, FFR is defined as the ratio of time-averaged distal coronary pressure to aortic pressure^{16,17}

$$FFR = \frac{\tilde{p}_d}{\tilde{p}_a} = 1 - \frac{\Delta\tilde{p}}{\tilde{p}_a} \tag{6}$$

Statistical analysis

Haemodynamic data were collected as continuous and categorical from the numerical study. The \tilde{p}_a , $\Delta\tilde{p}$ and FFR obtained from all configurations were entered into SPSS 22.0 (SPSS, Inc., Chicago, IL, USA) for statistical analysis. A *p*-value of <0.05 was considered statistically significant. A one-way ANOVA between groups was used for analysis of haemodynamic data to determine differences between BA and FDV in CAB.

Results

Effect of angulation and flow through CAB on pressure and FFR

Type (1, 0, 0): For the lesion type (1, 0, 0), results showed a significant difference in $\Delta\tilde{p}$ (Figure 5) and FFR (*p* > 0.05) and no significant difference in \tilde{p}_a (*p* < 0.05) as BA gradually varied from 30° to 120°, for any fixed flow through LAD. However, as flow through LAD var-

ied, a significant difference was found in \tilde{p}_a (*p* < 0.05) and FFR (*p* < 0.05), and no significant difference in $\Delta\tilde{p}$ for any fixed angulation model. Figure 6 shows the transient proximal pressure in 75° bifurcated angulation model under different percentage of FD in LAD.

For a given stenosis severity, \tilde{p}_a ranged from 91.82 to 106.02 mmHg, $\Delta\tilde{p}$ ranged from 14.3 to 16.38 mmHg and FFR ranged from 0.82 to 0.86, when flow through LAD ranged from 70% to 85% of \tilde{Q} for an angulation from 30° to 120° (Table 1). So, an overall 15% variation was found in \tilde{p}_a , 15% variation in $\Delta\tilde{p}$ and 5% variation in FFR.

Type (0, 1, 0): For (0, 1, 0) configuration, no significant difference was found in \tilde{p}_a , $\Delta\tilde{p}$ and FFR as BA gradually varied from 30° to 120°, for any fixed flow through a

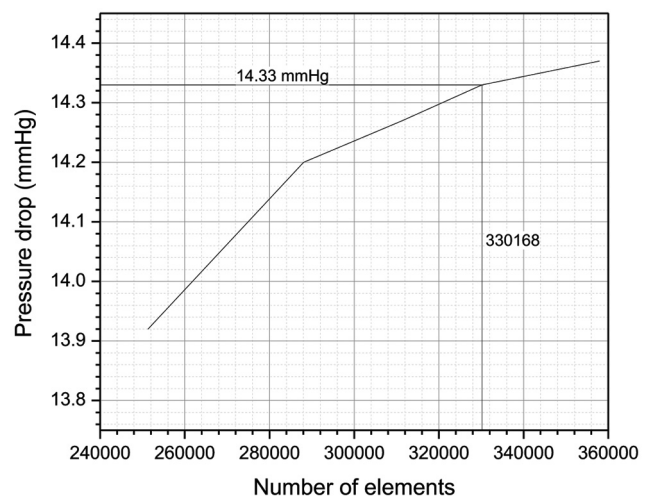


Figure 4. Mesh independency test for the model (1, 0, 0) of 75° bifurcation with 70% of \tilde{Q} through LAD.

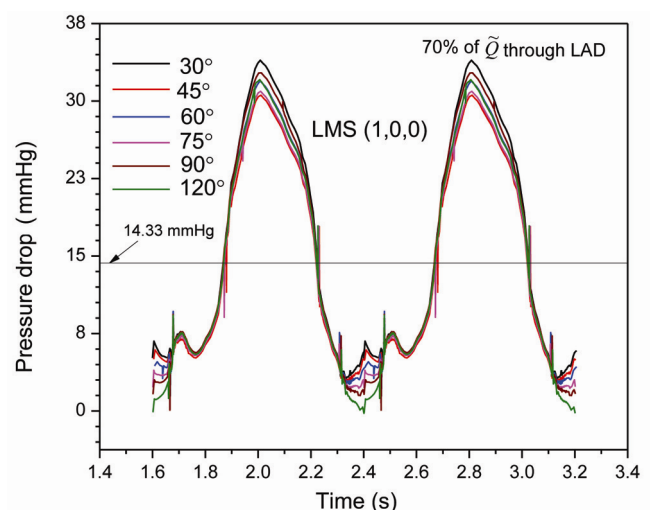


Figure 5. Transient pressure drop in the lesion type (1, 0, 0) under various bifurcated angulation model and $\Delta\tilde{p} = 14.33$ mmHg corresponds to 75° bifurcated artery model.

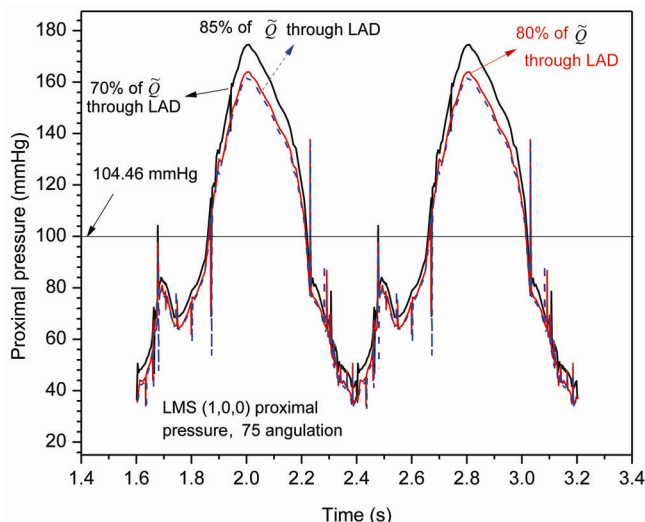


Figure 6. Transient proximal pressure in 75° bifurcated angulation model (1, 0, 0), under different percentage of FDV through LAD and $\bar{p}_a = 104.46$ mmHg corresponds to 70% of \dot{Q} .

LAD. However, as flow through the LAD varied, a significant difference was found in \bar{p}_a ($p < 0.05$), $\Delta\bar{p}$ ($p < 0.05$) and FFR ($p < 0.05$), for any fixed angulation model.

For a given stenosis severity, \bar{p}_a ranged from 91.06 to 99.83 mmHg, $\Delta\bar{p}$ ranged from 33.81 to 49.09 mmHg and FFR ranged from 0.46 to 0.65, when the flow through LAD ranged from 70% to 85% of \dot{Q} for an angulation ranged from 30° to 120° (Table 2). Overall 10% variation was found in \bar{p}_a , 45% in $\Delta\bar{p}$ and 41% in FFR.

Type (0, 0, 1): Lesion type (0, 0, 1) did not show any significance in \bar{p}_a , $\Delta\bar{p}$ and FFR as angulation varied from 30° to 120° for any fixed flow through LCX. However, as flow through LCX varied, there was a significant difference in \bar{p}_a ($p < 0.05$), $\Delta\bar{p}$ ($p < 0.05$) and FFR ($p < 0.05$) between the percentage of flow rates through LCX. For a given stenosis severity, \bar{p}_a ranged from 87.39 to 90.58 mmHg, $\Delta\bar{p}$ ranged from 15.1 to 45.53 mmHg and the FFR ranged from 0.48 to 0.83 when the flow through LAD was 20% to 40% of \dot{Q} for the angulation 30° to 120° (Table 3). Overall 4% variation was found in the \bar{p}_a , 202% in $\Delta\bar{p}$ and 73% in FFR.

Discussion

Clinical study indicated that PCI for coronary bifurcation lesions has been associated with higher procedural and restenosis rate, compared with simple coronary lesion. FFR is generally used in bifurcation lesions for clinical diagnosis. Coronary branch steal may overestimate or underestimate bifurcation lesion severity, when FFR was measured across branch stenosis^{33,34}. Despite the complexity of bifurcation lesions, previous studies³³⁻³⁵ have not focussed on quantitatively analysing the influence of

BA, ranging from narrow angle to wider angle which is a significant physiological condition and FDV in CAB. In this study, BA and percentage of FDV in CAB are the two important independent variables. The present results demonstrate that the variation of branch angle and percentage of FDV in CAB, significantly influence aortic pressure and/or pressure drop across the stenosis and hence alters the FFR in the bifurcated artery lesions where coronary intervention is often controversial. This seems to be the first numerical study to investigate variations in the FFR in bifurcated lesion, in the context of Medina classification, by considering BA and percentage of FDV in CAB.

Bifurcated artery with fixed percentage of FD in CAB and variable angulation on FFR

Our results demonstrated that for a given percentage of AS and fixed percentage of FD in CAB in the lesion type (1, 0, 0), BA variations have no significant effect on proximal pressure, despite the influence of angulation of the artery on the pressure drop. For the given severity condition, pressure drop was significantly lower in the wide-angled model than the narrow-angled model and hence FFR showed a higher value in the wide-angled model and vice versa. Fractional flow reserve is indirectly related to pressure drop across the stenosis, provided that aortic pressure is constant during measurement. Hence the wide-angled stenosed bifurcated artery shows higher FFR than the narrow-angled stenosed bifurcated artery. For lesion types (0, 1, 0) and (0, 0, 1), no significant changes were found in the pressure drop/aortic pressure and hence the FFR, as BA varied. The mean \pm SD value of FFR for the bifurcation type (1, 0, 0) was 0.85 ± 0.01 and it was in close agreement with the previous studies (Table 4)^{23,25}. The threshold of FFR is determined in a large patient study^{36,37}, so the BA is already incorporated in this threshold. Nevertheless, measuring FFR in bifurcated artery may lead to misjudgement of the plaque severity and a correction may be applied when FFR value of 0.80 is obtained.

The significant FFR variation caused by arterial BA in lesion type (1, 0, 0) will notably affect the anatomical assessment of intermediate stenosis. From the clinical study by Kristensen *et al.*³⁸, percentage of AS obtained from coronary computed tomography angiography appears to be clinically useful and is significantly correlated with FFR. Hence the influence of BA should not be ignored in the lesion type (1, 0, 0) when assessing stenosis severity non-invasively as an alternative to FFR.

Percentage of FDV in CAB on the FFR with any fixed angulation

Results showed that for any given angulation, the percentage of FDV in CAB significantly affects the FFR in all lesion

Table 1. Results from computational analysis (1, 0, 0)

Angulation (θ)	70% of \tilde{Q}			80% of \tilde{Q}			85% of \tilde{Q}		
	\bar{p}_a (mmHg)	$\Delta\bar{p}$ (mmHg)	FFR	\bar{p}_a (mmHg)	$\Delta\bar{p}$ (mmHg)	FFR	\bar{p}_a (mmHg)	$\Delta\bar{p}$ (mmHg)	FFR
30	98.69	15.85	0.84	92.87	16.28	0.83	91.82	16.38	0.82
45	100.1	14.3	0.86	94.51	14.74	0.84	93.28	14.83	0.84
60	104.31	14.87	0.86	97.85	15.23	0.84	96.66	15.34	0.84
75	104.46	14.33	0.86	98.09	14.62	0.85	96.45	14.61	0.85
90	106.02	15.05	0.86	100.22	15.82	0.84	98.41	15.81	0.84
120	105.46	14.39	0.86	98.89	14.57	0.85	97.39	14.61	0.85

Table 2. Results from computational analysis (0, 1, 0)

Angulation (θ)	70% of \tilde{Q}			80% of \tilde{Q}			85% of \tilde{Q}		
	\bar{p}_a (mmHg)	$\Delta\bar{p}$ (mmHg)	FFR	\bar{p}_a (mmHg)	$\Delta\bar{p}$ (mmHg)	FFR	\bar{p}_a (mmHg)	$\Delta\bar{p}$ (mmHg)	FFR
30	97.20	35.11	0.64	92.15	45.88	0.5	91.06	49.09	0.46
45	97.29	33.81	0.65	92.1	44.3	0.52	91.16	47.03	0.48
60	97.24	34.43	0.65	92.35	45.21	0.51	91.27	47.81	0.48
75	97.71	34.47	0.65	92.87	45.42	0.52	91.96	48.35	0.47
90	98.74	34.7	0.65	93.56	45.68	0.51	92.18	48.23	0.48
120	99.83	34.73	0.65	95.14	48.66	0.51	93.49	48.85	0.48

Table 3. Results from computational analysis (0, 0, 1)

Angulation (θ)	20% of \tilde{Q}			30% of \tilde{Q}			40% of \tilde{Q}		
	\bar{p}_a (mmHg)	$\Delta\bar{p}$ (mmHg)	FFR	\bar{p}_a (mmHg)	$\Delta\bar{p}$ (mmHg)	FFR	\bar{p}_a (mmHg)	$\Delta\bar{p}$ (mmHg)	FFR
30	90.51	15.29	0.83	88.97	27.65	0.69	87.64	41.38	0.53
45	90.29	15.91	0.82	88.78	28.86	0.68	87.41	43.38	0.50
60	90.36	15.1	0.83	88.83	27.44	0.69	87.59	41.33	0.53
75	90.46	15.54	0.83	88.92	28.3	0.68	87.45	42.53	0.51
90	90.58	16.22	0.82	89.02	29.59	0.67	87.63	41.58	0.53
120	90.26	16.54	0.82	88.74	30.27	0.66	87.39	45.53	0.48

Table 4. Comparison of our $\Delta\bar{p}$ and FFR value for the model (1, 0, 0) with previous study

	Roy <i>et al.</i> ²⁵	Konala <i>et al.</i> ²³	Present study
$\Delta\bar{p}$ (mm Hg)	14.3	20	15.09 \pm 0.64
FFR	0.82	0.78	0.85 \pm 0.01

types. For configurations (1, 0, 0) and (0, 1, 0), if the flow through LAD decreases, the measured FFR will increase and for the configuration (0, 0, 1), if the flow through LCX decreases, the FFR will also increase. The measured FFR in each configuration might lead to misinterpretation of intermediate stenosis, unless a prior knowledge of LCA branch flow is available. A lack of knowledge of branch flow and its effect on FFR might wrongly lead to the postponement of coronary interventional procedures, particularly in patients with intermediate stenosis.

Some significant limitations of this study are the factors that influence diagnostic parameters, such as arterial wall compliance²³, multiple bend, and dynamic curvature variation caused by heart motion³⁹, wall roughness, and lesion eccentricity, were not considered. However, our

results are useful in the research design of future studies, using realistic coronary artery model, which will address current limitations in the analysis of influence of BA and CAB flow on stenosis severity.

Conclusion

This numerical study analysed the influence of bifurcated coronary artery wall angulation and CAB flow, in order to investigate the FFR variation in the LCA, according to Medina classification. The results show that variation in BA significantly altered FFR in the lesion type (1, 0, 0) and it could be considered addition to minimum lumen area/percentage of area stenosis in the non-invasive assessment of stenosis severity as an alternative to FFR, whereas, in the lesion types (0, 1, 0) and (0, 0, 1) BA variations are non-significant. The percentage of FDV in CAB significantly altered FFR for the same severity of stenosis in all lesion types for a given BA. In case of intermediate stenosis, coronary branch steal underestimates the stenosis severity, resulting in postponement of coronary interventional procedure. Our mathematical model demonstrates the proof of concept that needs to be tested

in human arteries. However, further *in vivo* and *in vitro* studies and validations are required to correlate the anatomical and functional significance of stenosis severity.

1. Chaichana, T., Sun, Z. and Jewkes, J., Computation of hemodynamics in the left coronary artery with variable angulations. *J. Biomech.*, 2011, **44**, 1869–1878.
2. Wiwatanapataphee, B. *et al.*, Effect of branchings on blood flow in the system of human coronary arteries. *Math. Biosci. Eng.*, 2012, **9**, 199–214.
3. Giannoglou, G. D. *et al.*, Flow and atherosclerosis in coronary bifurcations. *EuroIntervention*, 2010, **6**, J16–J23.
4. Politis, A. K. *et al.*, Numerical modelling of simulated blood flow in idealized composite arterial coronary grafts: Transient flow. *J. Biomech.*, 2008, **41**, 25–39.
5. Tanboga, I. H. *et al.*, Reproducibility of syntax score: from core lab to real world. *J. Int. Cardiol.*, 2011, **24**, 302–306.
6. Medina, A., Suarez de Lezo, J. and Pan, M., A new classification of coronary bifurcation lesions. *Rev. Esp. Cardiol.*, 2006, **59**, 183.
7. Molavi Zarandi, M., Mongrain, R. and Bertrand, O. F., Determination of flow conditions in coronary bifurcation lesions in the context of the Medina classification. *Modelling Simul. Eng.*, 2012, **2012**, 1–10.
8. Chaichana, T., Sun, Z. and Jewkes, J., Hemodynamic impacts of various types of stenosis in the left coronary artery bifurcation: a patient-specific analysis. *Phys. Med.*, 2013, **29**, 447–452.
9. Chaichana, T., Sun, Z. and Jewkes, J., Haemodynamic analysis of the effect of different types of plaques in the left coronary artery. *Comput. Med. Imaging Graph.*, 2013, **37**, 197–206.
10. Murray, C. D., The physiological principle of minimum work applied to the angle of branching of arteries. *J. Gen. Physiol.*, 1926, **9**, 835–841.
11. Groen, H. C. *et al.*, Mri-based quantification of outflow boundary conditions for computational fluid dynamics of stenosed human carotid arteries. *J. Biomech.*, 2010, **43**, 2332–2338.
12. Park, S. H. and Koo, B. K., Clinical applications of fractional flow reserve in bifurcation lesions. *J. Geriatr. Cardiol.*, 2012, **9**, 278–284.
13. Ziaee, A. *et al.*, Lack of relation between imaging and physiology in ostial coronary artery narrowings. *Am. J. Cardiol.*, 2004, **93**, 1404–1407, A1409.
14. Tobis, J., Azarbal, B. and Slavin, L., Assessment of intermediate severity coronary lesions in the catheterization laboratory. *J. Am. Coll. Cardiol.*, 2007, **49**, 839–848.
15. Koo, B.-K. *et al.*, Physiologic assessment of jailed side branch lesions using fractional flow reserve. *J. Am. Coll. Cardiol.*, 2005, **46**, 633–637.
16. Pijls, N. H. J. and Sels, J.-W. E. M., Functional measurement of coronary stenosis. *J. Am. Coll. Cardiol.*, 2012, **59**, 1045–1057.
17. Pijls, N. H. *et al.*, Fractional flow reserve. A useful index to evaluate the influence of an epicardial coronary stenosis on myocardial blood flow. *Circulation*, 1995, **92**, 3183–3193.
18. Melikian, N. *et al.*, Fractional flow reserve and myocardial perfusion imaging in patients with angiographic multivessel coronary artery disease. *JACC: Cardiovasc. Interv.*, 2010, **3**, 307–314.
19. Dong, J., Fluid–structure interaction analysis of the left coronary artery with variable angulation. *Comput. Meth. Biomech. Biomed. Eng.*, 2014, **18**, 1–9.
20. Dash, R. K., Jayaraman, G. and Mehta, K. N., Flow in a catheterized curved artery with stenosis. *J. Biomech.*, 1999, **32**, 49–61.
21. Brosh, D., *et al.*, Effect of lesion length on fractional flow reserve in intermediate coronary lesions. *Am. Heart J.*, 2005, **150**, 338–343.
22. Cho, Y. I. and Kensey, K. R., Effects of the non-newtonian viscosity of blood on flows in a diseased arterial vessel. Part 1: steady flows. *Biorheology*, 1991, **28**, 241–262.
23. Konala, B. C., Das, A. and Banerjee, R. K., Influence of arterial wall-stenosis compliance on the coronary diagnostic parameters. *J. Biomech.*, 2011, **44**, 842–847.
24. Cho, Y. I. *et al.*, Experimental study of pulsatile and steady flow through a smooth tube and an atherosclerotic coronary artery casting of man. *J. Biomech.*, 1983, **16**, 933–946.
25. Roy, A. S. *et al.*, Delineating the guide-wire flow obstruction effect in assessment of fractional flow reserve and coronary flow reserve measurements. *Am. J. Physiol. Heart Circ. Physiol.*, 2005, **289**, H392–H397.
26. Wilson, R. F., Marcus, M. L. and White, C. W., Prediction of the physiologic significance of coronary arterial lesions by quantitative lesion geometry in patients with limited coronary artery disease. *Circulation*, 1987, **75**, 723–732.
27. Wilson, R. F. *et al.*, The effect of coronary angioplasty on coronary flow reserve. *Circulation*, 1988, **77**, 873–885.
28. Taylor, C. A., Hughes, T. J. R. and Zarins, C. K., Finite element modeling of blood flow in arteries. *Comput. Meth. Appl. Mech. Eng.*, 1998, **158**, 155–196.
29. Ansys cfx-solver modeling guide, ANSYS 14, 2011.
30. Govindaraju, K. *et al.*, Effect of porous media of the stenosed artery wall to the coronary physiological diagnostic parameter: A computational fluid dynamic analysis. *Atherosclerosis*, 2014, **233**, 630–635.
31. Banerjee, R. K. *et al.*, Hemodynamic diagnostics of epicardial coronary stenoses: *in vitro* experimental and computational study. *Biomed. Eng. Online*, 2008, **7**, 24.
32. Sabik, J. F. *et al.*, Does competitive flow reduce internal thoracic artery graft patency? *Ann. Thoracic Surg.*, 2003, **76**, 1490–1497.
33. Koo, B. K., Physiologic evaluation of bifurcation lesions using fractional flow reserve. *J. Interv. Cardiol.*, 2009, **22**, 110–113.
34. Gould, K. L., Kirkeeide, R. and Johnson, N. P., Coronary branch steal: experimental validation and clinical implications of interacting stenosis in branching coronary arteries. *Circ. Cardiovasc. Imaging*, 2010, **3**, 701–709.
35. Sarno, G. *et al.*, Bifurcation lesions: functional assessment by fractional flow reserve vs anatomical assessment using conventional and dedicated bifurcation quantitative coronary angiogram. *Catheter. Cardiovasc. Interv.*, 2010, **76**, 817–823.
36. Pijls, N. H. J. *et al.*, Percutaneous coronary intervention of functionally nonsignificant stenosis: 5-year follow-up of the defer study. *J. Am. College Cardiol.*, 2007, **49**, 2105–2111.
37. Pijls, N. H. J. *et al.*, Fractional flow reserve versus angiography for guiding percutaneous coronary intervention in patients with multivessel coronary artery disease: 2-year follow-up of the fame (fractional flow reserve versus angiography for multivessel evaluation) study. *J. Am. Coll. Cardiol.*, 2010, **56**, 177–184.
38. Kristensen, T. S. *et al.*, Correlation between coronary computed tomographic angiography and fractional flow reserve. *Int. J. Cardiol.*, 2010, **144**, 200–205.
39. Yang, C. *et al.*, Cyclic bending contributes to high stress in a human coronary atherosclerotic plaque and rupture risk: *in vitro* experimental modeling and *ex vivo* mri-based computational modeling approach. *Mol. Cell Biomech.*, 2008, **5**, 259–274.

ACKNOWLEDGEMENT. We thank University of Malaya for funding the research under the grant number RP006A-13AET and PG212-2015B. We acknowledge the facilities provided by HELP College of Arts and Technology (HELP CAT), a member of the HELP Group. Thanks to Meenadevi Govindaraju for helping our research activities.

Received 6 May 2015; revised accepted 9 March 2016

doi: 10.18520/cs/v111/i2/368-374